SOILS AND FOUNDATIONS Vol. 43, No. 5, 13-27, Oct. 2003
Japanese Geotechnical Society

BEHAVIORS OF SEVERAL TYPES OF MODEL RETAINING WALLS SUBJECTED TO IRREGULAR EXCITATION

KENJI WATANABE[i], YULMAN MUNAF[ii], JUNICHI KOSEKI[iii], MASARU TATEYAMA[iv] and KENICHI KOJIMA[iv]

ABSTRACT

In order to establish practical design procedures to evaluate seismic stability of different types of retaining walls against high seismic loads, a series of shaking table tests were conducted with irregular excitation on retaining wall models consisting of six different types. Reinforced-soil retaining wall models with a rigid full-height facing exhibited a ductile behavior, when compared with conventional type retaining wall models such as gravity, leaning and cantilever-types. When the conventional type wall started to tilt, the subsoil reaction force at the toe of wall suddenly decreased due to the loss of bearing capacity. On the other hand, under similar conditions, the tensile force in the reinforcement of reinforced-soil walls could be mobilized effectively to resist overturning.

Key words: bearing capacity, (failure plane), reinforced soil, retaining wall, (seismic earth pressure), shaking table test (**IGC**: E5/E8)

INTRODUCTION

In recent years, there has been serious damage to retaining walls (RWs) due to large earthquakes. The Hyogoken-Nambu earthquake on January 17, 1995, for example, caused serious damage to conventional masonry and concrete gravity-type RWs for railway embankments. On the other hand, the reinforced-soil RWs exhibited a ductile behavior and did not reach critical failure as reported by Tatsuoka et al. (1996).

The forces acting on RWs during an earthquake are inertia force, subsoil reaction, seismic earth pressure and tensile force in the reinforcement as schematically shown in Fig. 1. The subsoil reaction and the seismic earth pressure are affected by the dynamic interaction between the wall and the subsoil/backfill, of which detailed mechanisms have not yet been clarified well. Furthermore, for reinforced-soil RWs, the interaction between the soil and the reinforcement, the seismic behavior of the reinforced or unreinforced zones of the backfill have also not yet been clarified in detail. For these reasons, it is difficult to predict the seismic behavior of RWs rationally.

It should also be noted that, in the current aseismic design procedures based on the pseudo-static approach, the different extents of ductility and seismic performance of different types of RWs have not been taken into account properly.

After the Hyogoken-Nambu earthquake, it was suggested that values of the seismic coefficient $(k_h)_{design}$ used in the current aseismic design procedures should be increased appropriately. In order to set the seismic coefficient appropriately, it is necessary to evaluate the different extents of ductility among different types of RWs and investigate the detail failure mechanism of RWs during an earthquake.

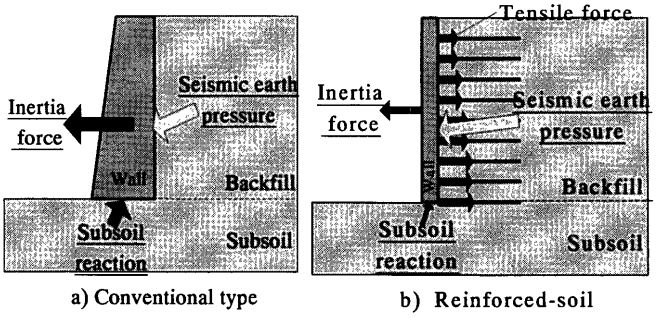

Fig. 1. Forces acting on retaining walls during earthquake

Shaking table tests on small-scale models of conventional type retaining walls and geosynthetic-reinforced soil retaining walls were conducted by several researchers as summarized by Whitman (1990) and Bathurst et al. (1996), respectively. However, their seismic behavior has not been compared with that of other types of retaining walls; Sakaguchi (1996) compared the dynamic stability

[i] Railway Technical Research Institute, Japan (nabeken@rtri.or.jp)
[ii] formerly Department of Civil Engineering, University of Tokyo
[iii] Institute of Industrial Science, University of Tokyo, Japan
[iv] Railway Technical Research Institute, Japan
Manuscript was received for review on April 18, 2002.
Written discussions on this paper should be submitted before May 1, 2004 to the Japanese Geotechnical Society, Sugayama Bldg. 4F, Kanda Awaji-cho 2-23, Chiyoda-ku, Tokyo 101-0063, Japan. Upon request the closing date may be extended one month.

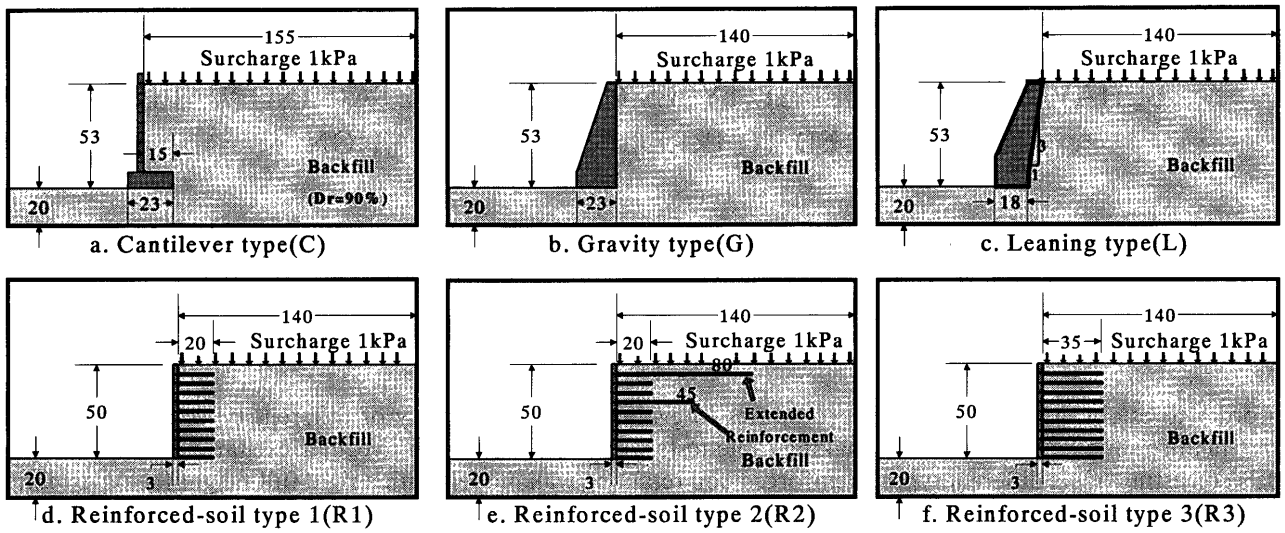

Fig. 2. Cross-section of model retaining walls (unit in cm)

of a geogrid-reinforced soil retaining wall having wrapped-around facing with that of conventional-type (gravity-type, leaning-type, and cantilever-type) retaining wall models. In addition, most of the previous researches adopted sinusoidal excitation for shaking table tests, and the seismic behavior of retaining walls subjected to different types of excitation was not compared.

In this study, therefore, a series of relatively small-scale model tests were conducted on different types of RWs to compare their performance during irregular shaking. The results from irregular shaking tests were compared with those from tilting tests and sinusoidal shaking tests that used the same RW models as reported by Koseki et al. (1998a, 1999).

TESTING PROCEDURES

Model of Retaining Wall and Backfill

The model tests were conducted by using a shaking table at the Railway Technical Research Institute, Japan. A rigid soil container (260 cm long, 60 cm wide, and 140 cm high) was fixed to this table.

Figure 2 shows the cross-sections of six different model retaining walls. The models were 600 mm in width (Fig. 3). They consisted of three conventional RWs (cantilever type, gravity type and leaning type) and three types of reinforced-soil RWs with a full-height rigid facing having different arrangements of reinforcement layers (reinforced-soil type 1, type 2 and type 3 RWs). The geometric shape of these models was set by referring to that of typical ones having a height of about 5 m in Japan, while reducing their size to a scale of almost one-tenth. The total height of the conventional walls was 530 mm, while that of the reinforced-soil walls was 500 mm. The bottom width at the base of the cantilever and gravity type walls was 230 mm, while it was reduced to 180 mm for the leaning type wall. In addition, in order to adjust the self weight of the gravity type and the leaning type walls, extra weights were added near the center

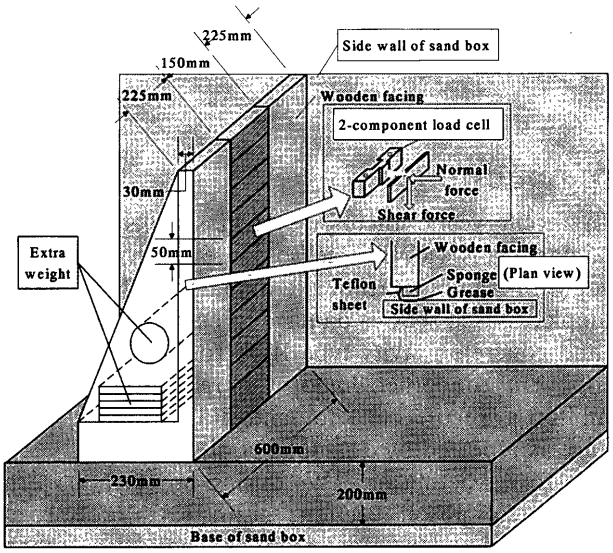

Fig. 3. Details of gravity type wall model

of gravity of these walls. The total amount of these extra weights was set so that the minimum of critical seismic coefficient of each retaining wall yielding a safety factor of unity against sliding, overturning and bearing capacity failure falls in the range from 0.3 to 0.4, when the relevant design procedures followed the limit-equilibrium and pseudo-static approach. Further, the total weight of the gravity type wall was adjusted to be larger than that of the cantilever type wall including the weight of backfill located above its base footing. Koseki et al. (1998a) have described the details of this model wall.

For the reinforced-soil RW models, a grid of phosphor-bronze strips was used as the model reinforcement. To form a lattice-shaped layer of model reinforcement, strips having a thickness of 0.1 mm and a width of 3 mm were soldered to each other at intervals of 50 mm in the direction parallel to the side wall and 100 mm in the direction normal to it, as shown in Fig. 4. To effectively mobilize friction between the reinforcement and the backfill,

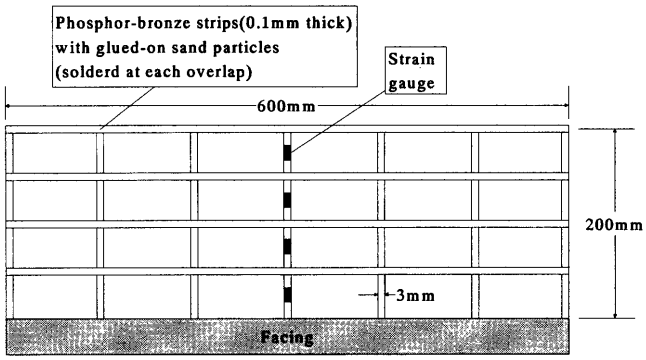

Fig. 4. Plan of model reinforcement layer

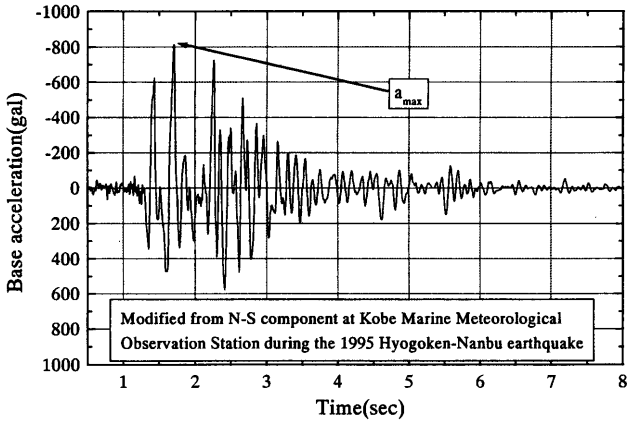

Fig. 5. Typical time history of base acceleration

sand particles were glued on the surface of the strips. Ten layers of reinforcement strips were horizontally placed at a vertical spacing of 50 mm in the backfill for all reinforced-soil RWs. This vertical spacing was set by reducing them to a scale of nearly one-tenth that of actual reinforced soil retaining walls with a full-height rigid facing constructed in Japan (R.T.R.I., 2000a). For the reinforced-soil type 1 RW, the length of all reinforcements (200 mm) was determined so that the sum of the reinforcement length and the wall width becomes equal to the width of the base footing of the cantilever and gravity type walls (230 mm). The length of the top and the fourth reinforcement layers were increased to 800 mm and 450 mm, respectively, for the reinforced-soil type 2 RW in order to increase the stability against overturning failure, as is the common practice in Japan. To study the effects of the length of reinforcement layers, the lengths of all reinforcement layers were increased to 350 mm for the reinforced-soil type 3 RW. Strain gauges were attached to the reinforcements to measure the tensile force. Note that the geometric shape and the arrangement of reinforcement model were determined by referring to those of actual ones, while the differences in the strength and deformation characteristics of model and actual reinforcements were not considered in this study. The tensile failure of reinforcements and the possible effects of deformation of reinforcements were outside the scope of this study.

The subsoil and the backfill layers were made of air-dried Toyoura sand ($D_{50}=0.23$ mm, $G_s=2.648$, $e_{max}=0.977$ and $e_{min}=0.609$). The sand layers were prepared by using a sand hopper and keeping the falling height of sand particles constant. The average relative density of 90% was achieved by this method.

In order to minimize the friction between the edge of RW models and the side wall of the soil container, a sponge, Teflon sheet and grease were used as schematically shown in Fig. 3. The leakage of the sand from the gap between RW models and the soil container could completely be prevented by this method.

To observe the deformation and displacement of sand layers, horizontal layers of black-dyed Toyoura sand having a thickness of 10 mm were prepared at a vertical spacing of 50 mm adjacent to the transparent side wall of the soil container as well as along the center line of the soil container.

After filling the sand, the surface of the backfill was trimmed to the prescribed geometry, and a surcharge of 1 kPa was applied by placing lead shots on the surface of the backfill.

The seismic earth pressure acting on the backface of the wall and the subsoil reaction at the bottom of the base footing were monitored by using two-component load cells which can record both the normal and shear components of earth pressure as shown in Fig. 3. The load cells were placed along the center line of the wall surface in order to reduce the effects of the side wall friction of the soil container. The results from analyses of measured seismic earth pressures will be shown elsewhere.

To measure the response of each retaining wall and backfill, a number of displacement transducers and accelerometers were installed.

Shaking Table Tests

Seismic loads were applied by shaking the soil container horizontally by means of irregular base acceleration. A strong motion that was recorded as an N-S component at Kobe Marine Meteorological Observation Station during the 1995 Hyogoken-Nambu earthquake was used as the base acceleration (Fig. 5). Its amplitude and time scale were adjusted so that the base acceleration had a prescribed maximum amplitude with a predominant frequency of 5 Hz. This predominant frequency was evaluated based on the Fourier spectrum of the base acceleration. Each model was subjected to several shaking steps, where the maximum amplitude of the base acceleration was initially set at 100 gals and increased at increments of 100 gals. Shaking was terminated when the wall displacement became considerably large.

Results from these irregular shaking tests were compared with the previous test results (Koseki et al., 1998a, 1999), where seismic loads were applied either by tilting the sand box to simulate pseudo-static loading conditions or by shaking the sand box with a sinusoidal base acceleration at a frequency of 5 Hz. In the tilting tests, the whole soil container was tilted continuously at a rate of approxi-

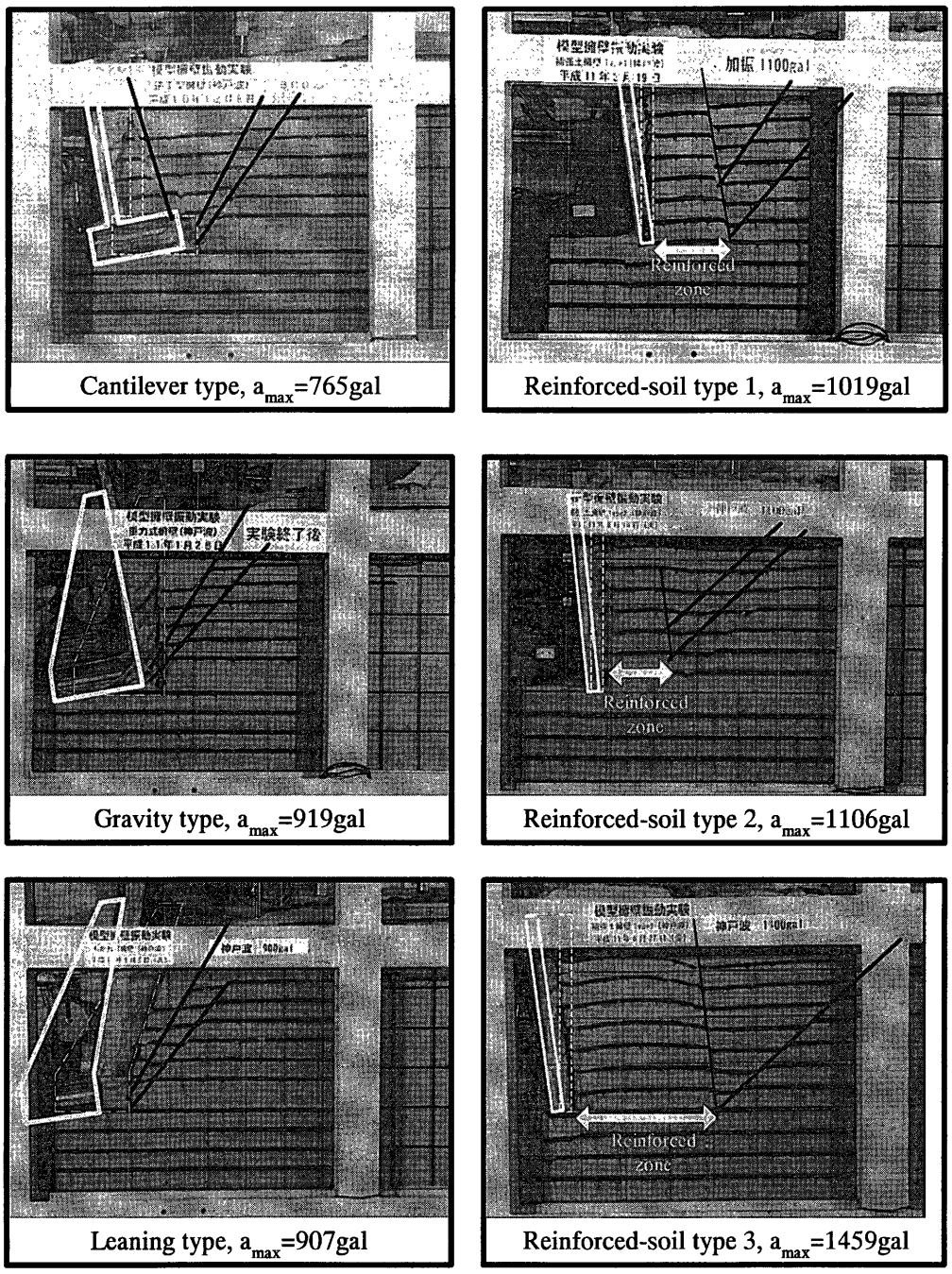

Fig. 6. Residual displacement of wall

mately 1.0 degree/minute. In the sinusoidal shaking tests, about 50 cycles of sinusoidal waves were applied as the base acceleration. The initial base acceleration was set first at 50 gal, and increased at increments of 50 gals.

TEST RESULTS AND DISCUSSION

Failure Pattern of Models

Figure 6 shows the residual displacement of the wall and the residual deformation of the backfill, which were observed at the end of the final shaking step.

For all RW models, the major failure pattern was overturning, which was associated with the bearing capacity failure of subsoil for the cantilever, leaning, and gravity type RWs. For these conventional type RWs, two differently inclined failure planes (plus a vertical failure plane starting from the heel of the wall in the case of the cantilever type RW) developed in the unreinforced backfill. For the cantilever type RW, two differently inclined failure planes developed almost simultaneously. On the other hand, for the leaning and gravity type RWs, the first failure plane developed much earlier than the second failure plane (Figs. 7(a) and 7(b)). This progressive formation of multiple failure planes can be explained by the effects of strain localization in the backfill soil and associated post-peak reduction in the shear resistance from the peak to residual values along a previously formed failure plane, as schematically shown in Fig. 8 and described in

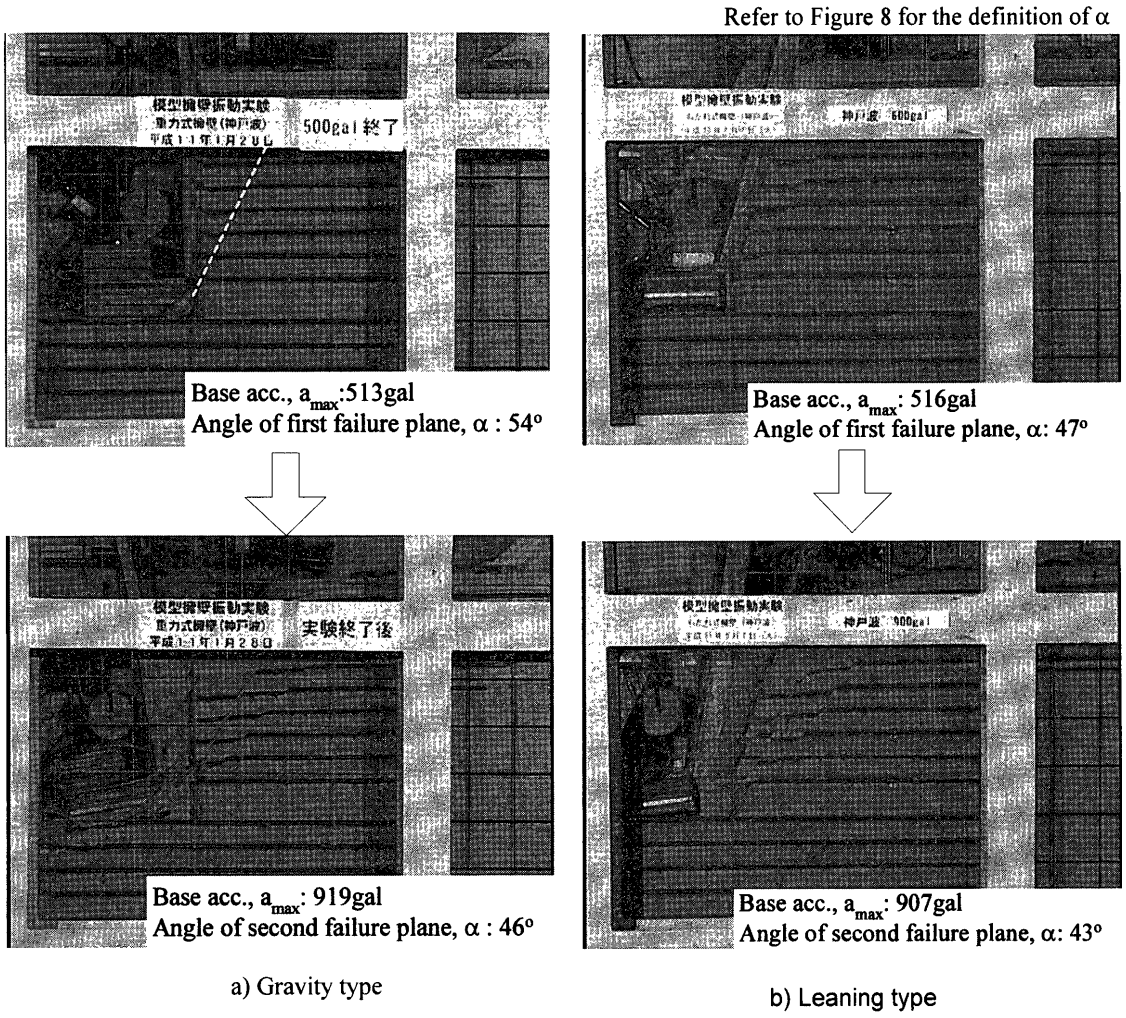

Fig. 7. Formation of first and second failure planes of gravity type and leaning type RW

detail by Koseki et al. (1998b). Such a behavior was not observed in the tilting tests or the sinusoidal shaking tests on the same RW models used in the present study, where localized shear displacements accumulated in the backfill only along a single failure plane (Koseki et al., 1998a). These different behaviors are possibly due to the difference in the duration of peak seismic load conditions. That is, in the case of tilting and sinusoidal shaking tests, as the duration of peak load conditions was longer than in irregular shaking tests, the wall suffered a large accumulation of residual displacement after it started to move outward, resulting in critical failure under relatively small seismic load conditions. Hence, a second failure plane which needs the application of larger seismic load was not formed in these tests. The detail of the relation between the residual displacement of the wall and the inertia force will be discussed later.

For the reinforced-soil RWs, two differently inclined failure planes developed almost simultaneously for the type 1 and type 2 walls, while only a single failure plane developed for the type 3 wall. For each wall, no failure planes were observed at the bottom of the front wedge in the reinforced zone. In the current seismic design procedure in Japan, a two-wedge failure mechanism which

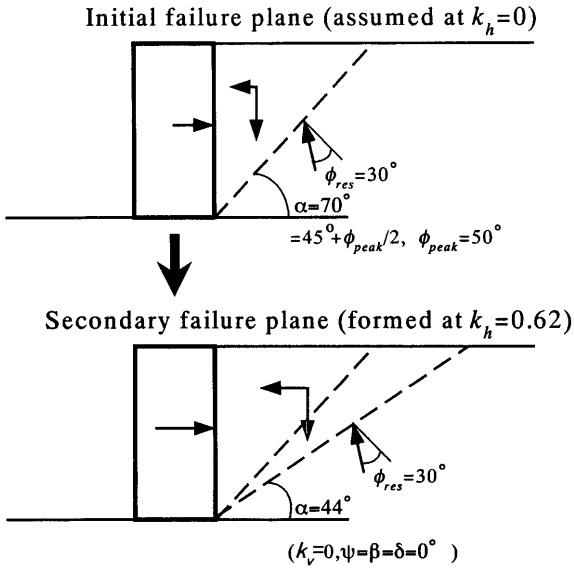

Fig. 8. Progressive formation of multiple failure planes considering effects of strain localization in backfill (after Koseki et al., 1998b)

assumes the front wedge and back wedge behave as a rigid body (Fig. 9) is often used in order to evaluate the stability of the reinforced-soil RWs (Horii et al., 1994). In the present shaking table tests, however, the front wedge did not behave as a rigid body, but it suffered simple shear deformation along horizontal planes. A similar behavior was observed in the tilting tests and the sinusoidal shaking tests (Koseki et al., 1998a). This behavior indicates that when the horizontal reinforcement is arranged sufficiently, the failure plane forms with difficulty through the reinforced backfill, while the horizontal reinforcement cannot effectively resist such simple shear deformation of the reinforced backfill. This simple shear deformation of the reinforced backfill should be considered in evaluating residual displacement of the wall properly, in particular for the reinforced-soil RWs with longer reinforcements.

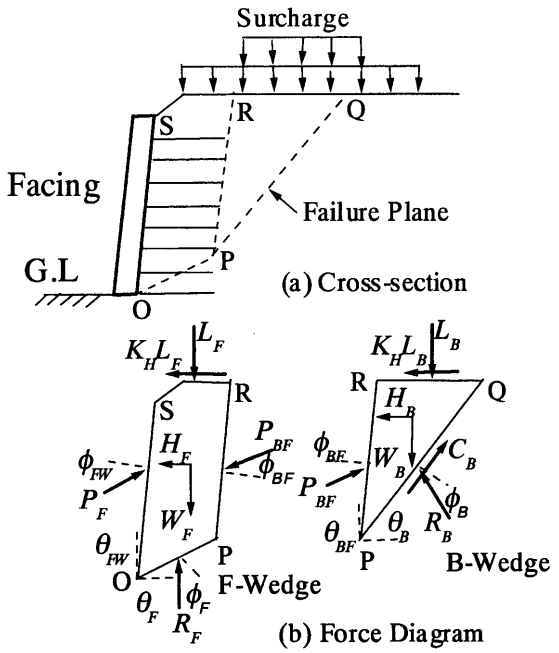

Fig. 9. Two wedge failure mechanism assumed in current seismic design of reinforced-soil retaining walls with rigid full-height facing (after Horii et al., 1994)

Residual Displacement of Wall

Figure 10 shows the relations between the seismic coefficient k_h and the residual wall top displacement $(d_{top})_{res}$. The value of $(d_{top})_{res}$, which is defined at the end of each shaking step, was measured at a height of 45 cm from the bottom of the base footing. Results from tilting and sinusoidal shaking tests (Koseki et al., 1998a, 1999) were also plotted. In the shaking tests, the seismic coefficient k_h was defined as $k_h = a_{max}/g$, where a_{max} is the maximum base acceleration at the active state (i.e., when the inertia force was oriented towards the active direction, Fig. 5) for each shaking step, and g is the gravitational acceleration. In the tilting tests, k_h was defined as $k_h = \tan\theta$, where θ is the tilting angle of the sand container. The residual wall top displacement at the same value of k_h was larger for the tests in the order of tilting test, sinusoidal shaking test and irregular shaking test. This is mainly due to the different duration of the peak seismic load among these three types of tests. That is, in the

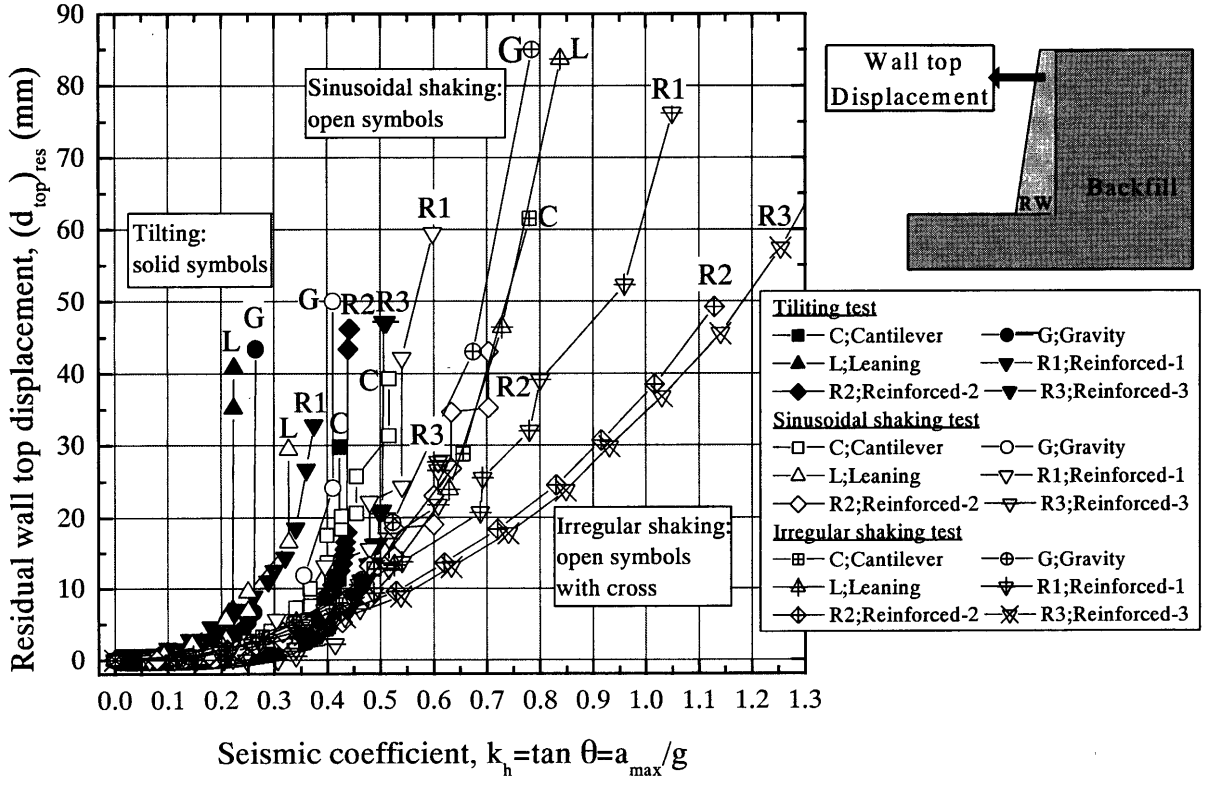

Fig. 10. Accumulation of residual horizontal displacement near the top of wall

tilting test, the external force which corresponds to the horizontal inertia force acts on the wall continuously throughout the tilting process. On the other hand, in the sinusoidal shaking test, the duration of the peak load condition at the active state was much shorter than that in the tilting test. Further, for the irregular shaking tests, the duration of peak load condition was quite limited (Fig. 5). Note that such comparison could be made for relatively low k_h value at which the failure did not occur in the tilting tests.

It can also be seen from Fig. 10 that in the early steps of irregular shaking tests up to a k_h value of about 0.5, the d_{top} value accumulated in a similar manner among different types of RWs. On the other hand, when the k_h value exceeded about 0.5, the rate of increase in the d_{top} value was larger for the conventional type RWs than for the reinforced-soil RWs. Further, though the total length of reinforcement of the type 2 wall was about 80% as large as that of the type 3 wall, their seismic stability were similar to each other.

Such different extents of ductility between conventional type RWs and reinforced-soil RWs agree qualitatively with the actual damage observed during the Hyogoken-Nanbu earthquake. This is caused by the different resistance mechanism against the external seismic forces acting on the wall. The details will be described later.

Displacement of Wall when a Failure Plane was Formed

Figure 11 shows the wall displacement $(d_{top})_{fp}$ which was measured at a height of 45 cm from the bottom of the base footing when a failure plane was formed in the backfill. The seismic coefficient $(k_h)_{fp}$ when the failure plane was formed in each test is also plotted in this figure. The following trends of behavior can be seen from this figure.

1) Although the failure plane was observed in a similar manner in the tilting tests as shown in Fig. 12, the wall displacement in the tilting tests when the failure plane was formed was much smaller than that in shaking table tests. This indicates that the condition of formation of failure plane under static loading is largely different from that under dynamic loading. Note that the displacement transducer was over-scaled in the sinusoidal shaking table test of reinforced-soil RW types 1 and 3. For the reinforced-soil RW type 1, the value of $(d_{top})_{fp}$ could be estimated because over-scaling occurred near the end of shaking.
2) The wall displacement in the sinusoidal shaking tests was similar to that in the irregular shaking tests except for the leaning type RW. This indicates that

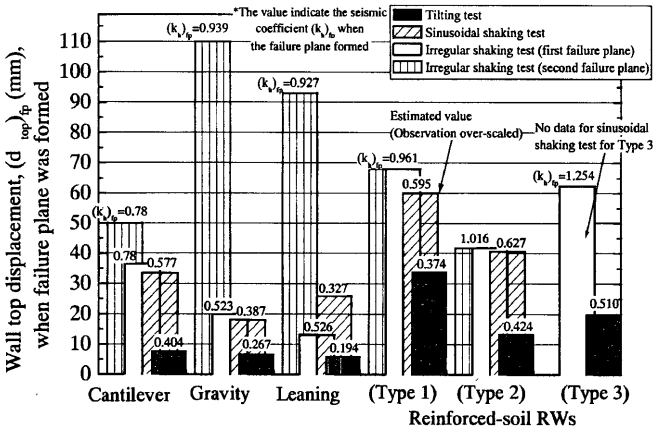

Fig. 11. Comparison of wall top displacements when a distinct failure plane was formed

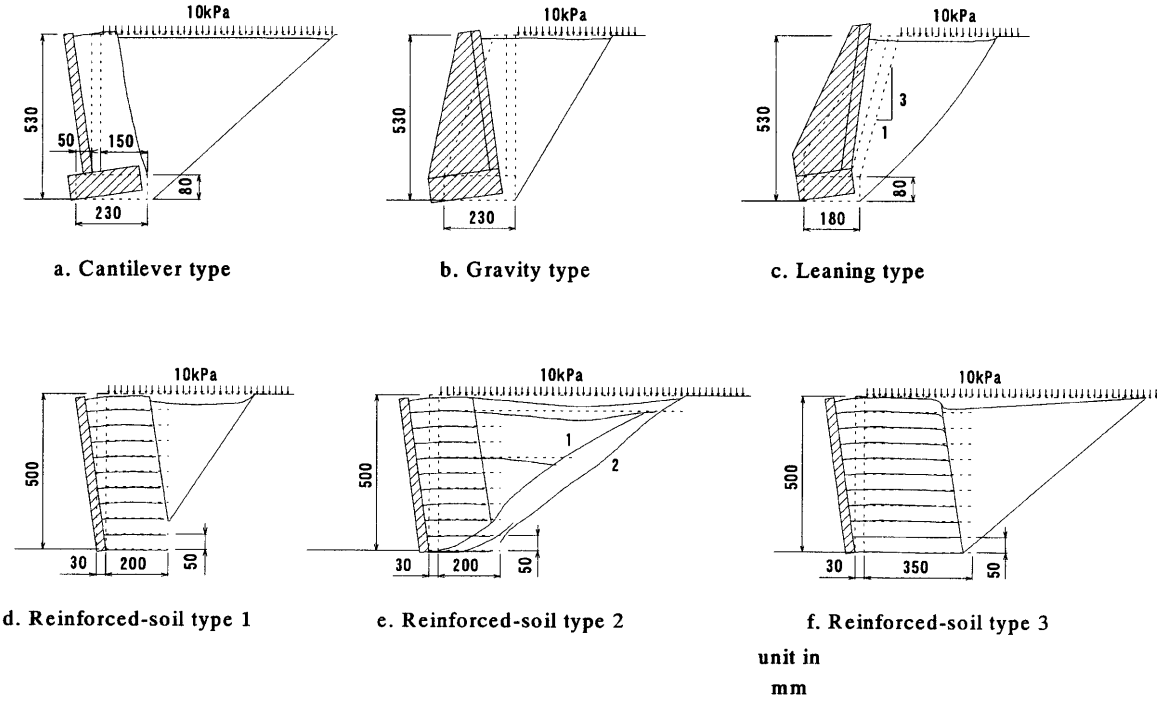

Fig. 12. Residual displacement of each wall after tilting test

when the predominant frequency of excitation was the same, the condition of formation of failure plane was not strongly influenced by the waveform.

3) The wall displacement of reinforced-soil RWs when the failure plane was formed was larger than that of conventional type RWs. Further, as shown in Fig. 6, the location of the failure plane was different between reinforced-soil RWs and conventional type RWs. These test results suggest that the condition of strain localization in the backfill is different between these two types of RWs. Further investigation is required on the condition of the strain localization in the backfill and the effect of loading condition on it.

Effect of Friction of Soil Container

The response acceleration, earth pressure and displacement were measured along the center line of the soil container (600 mm wide, Fig. 3) in order to reduce the influence of the side wall friction of the soil container as much as possible. During the process of removing backfill soil after the final shaking step, the angle of failure plane shown in Fig. 7 was also measured along the center line (*see* Fig. 24 for typical data). On the other hand, the moment of the formation of failure plane could be observed only through the transparent side wall of the sand container. The transparent side wall was made of glass, while the other side wall was made of steel covered with a Teflon sheet. In order to investigate the possible effect of the side wall friction, a special test was conducted on a gravity type RW model with sinusoidal excitation, where the response acceleration of the backfill and the moment of the formation of the failure plane were measured.

In this test, three accelerometers were set at the same depth and at the same distance from the back face of the RW as shown in Fig. 13. Figure 14 compares the maximum response acceleration in each shaking step. The maximum response accelerations were almost the same irrespective of the distance from the side wall, suggesting that the effect of the side wall friction on the response acceleration was not significant. It can also be seen from this figure that the response acceleration suddenly dropped when the base acceleration reached 440 gal and 530 gal. As the accelerometers were set above the failure plane this sudden drop of response acceleration would have been caused by the sliding of the backfill along the failure plane.

In order to detect the moment of the formation of failure plane in the backfill, electric sensors, schematically shown in Fig. 15, were set horizontally in the backfill where the failure plane was supposed to form. These sensors were made of very thin polyethylene which can be easily cut by a small extension force, on which conductive paint was pasted. Input voltage (about 5 volt) was constantly supplied and output voltage from this sensor was measured during shaking. When the sensor was cut by the formation of the failure plane, the output voltage suddenly decreased.

Figure 16 shows the time history of the output voltage

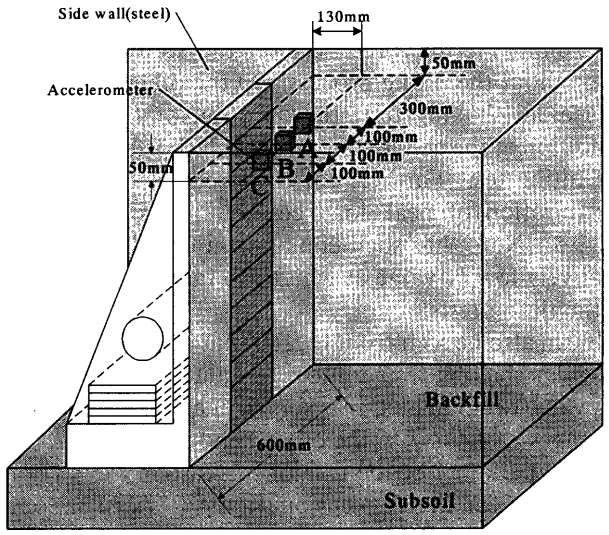

Fig. 13. Location of accelerometers to investigate effect of wall friction

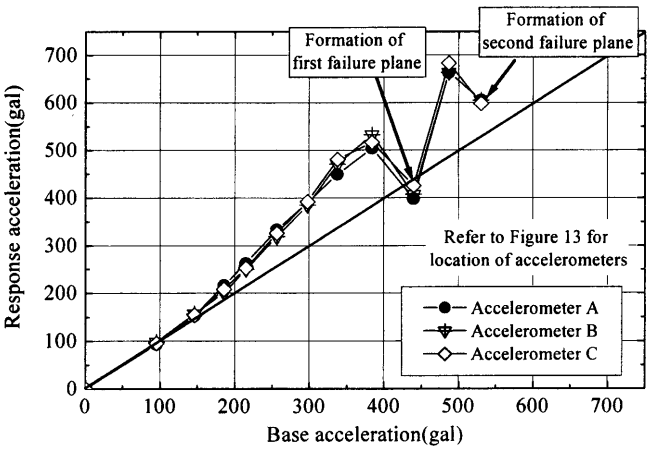

Fig. 14. Comparison of maximum response accelerations

of two electric sensors set along the center line of the soil container. One was set in the lower layer at the depth of 40 cm from the surface of the backfill, and the other was in the upper layer at a depth of 5 cm. In this figure, the moment of the formation of failure plane at the side wall is also shown, which was obtained by using a digital video camera that recorded the movement of the colored sand in the lower layer of the backfill through the transparent side wall. It can be seen from this figure that failure planes formed simultaneously in the lower layer of backfill near the transparent side wall and along the center line of the soil container.

On the other hand, the angle of failure plane measured from the horizontal direction was 54.0 degree along the center line, while it was 60.5 degree at the side wall. This indicates that the deformation pattern of backfill soil just beside the side wall was affected by the side wall friction to some extent. Based on these results, it was confirmed that, though the moment of the formation of failure plane could be determined by observing through the transparent side wall, the angle of failure plane should be

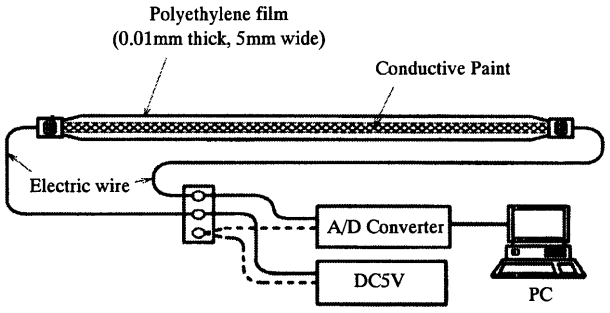

Fig. 15. Electric sensor to detect formation of failure plane

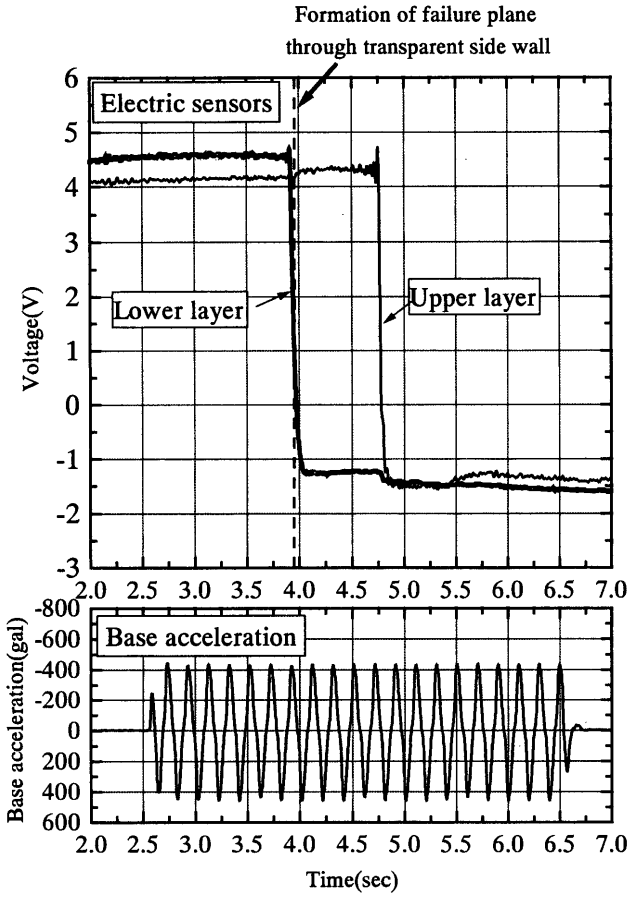

Fig. 16. Time history of electric sensor

measured along the center line of the soil container. Note that, since the accelerometer C in Fig. 13 was located at a horizontal distance of 100 mm from the side wall, its response was not significantly affected by the side wall friction.

It can also be seen from Fig. 16 that the electric sensor in the upper layer was cut about 0.7 seconds later than that in the lower layer, suggesting the occurrence of progressive failure of the backfill. Further investigations are required on this issue.

Seismic Stability of Conventional Type RWs

The different extents of ductility among different types of RWs, which is observed in Fig. 10, is discussed below,

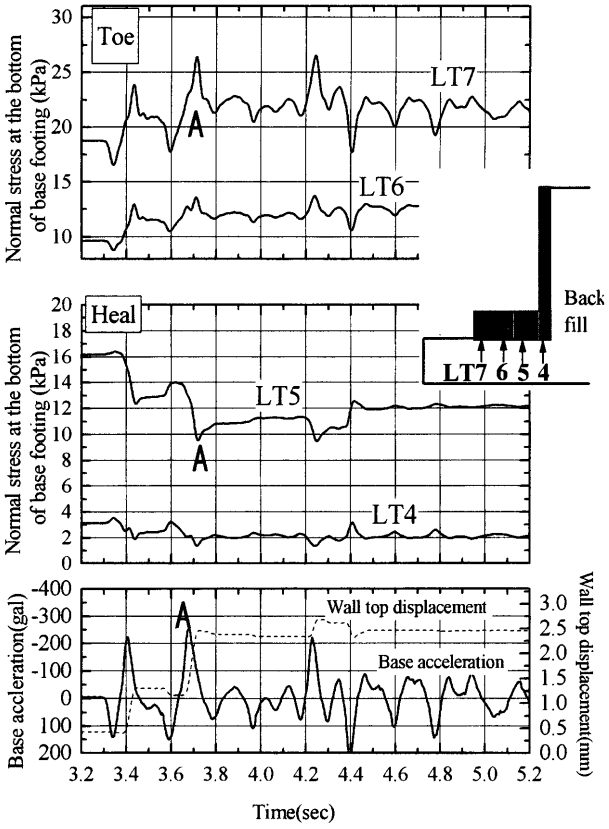

Fig. 17. Time history of normal component of subsoil reaction for gravity type retaining wall

focusing on their resistance mobilization against the external forces acting on the wall such as inertia force and seismic earth pressure.

The conventional type RWs resist overturning by the reaction force from subsoil, as shown in Fig. 1. Figure 17 shows the time history of the normal component of the reaction force which includes initial values measured before starting shaking for the gravity type RW. The reaction force was measured with four loadcells at the bottom of the base footing. When the inertia force was oriented outward (point A), the normal stress increased at the toe of the base footing, while it decreased at the heel. This behavior clearly revealed that overturning of the wall took place not around the toe of the footing but around an intermediate point located between the toe and the heel of the footing, causing stress concentration at the toe of the base footing. A similar tendency was observed for the cantilever type and leaning type RWs.

Figure 18 shows the relation between the normal reaction force from subsoil and the wall top horizontal displacement d_{top} for the gravity type RW. The reaction forces and its resultant value were evaluated when the base acceleration inducing an outward inertia force (active state) took the maximum value in each shaking step. Figure 19 shows the relation between the resultant normal force from the subsoil and relative location of its application point D/W. The parameter D denotes the distance between the application point of the resultant force

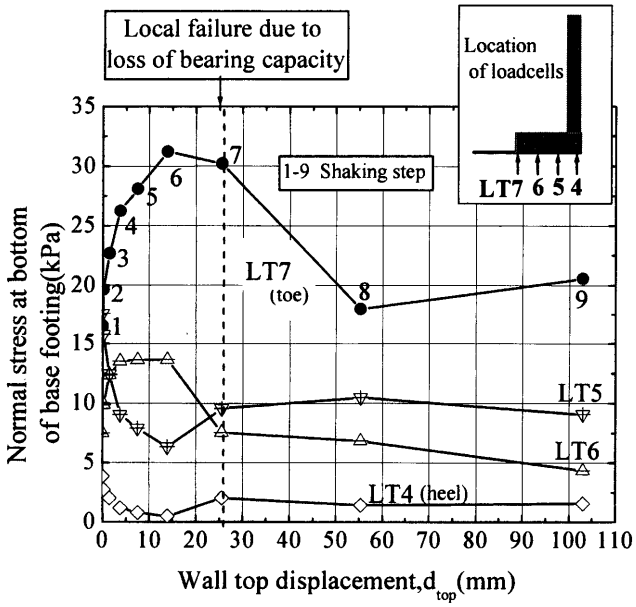

Fig. 18. Measured reactions from subsoil for gravity type retaining wall

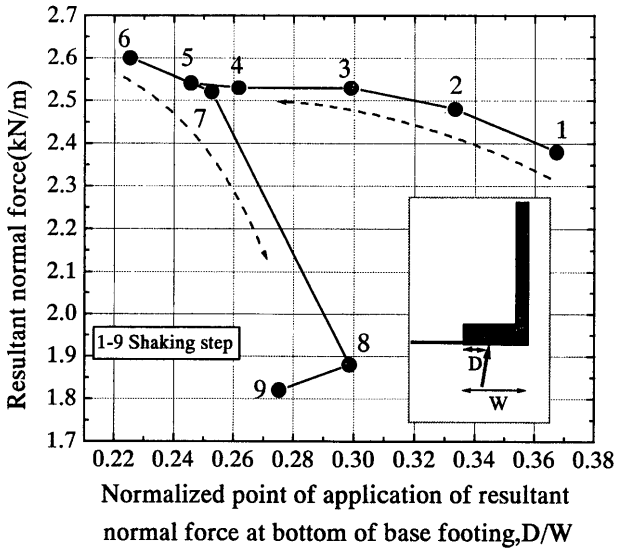

Fig. 19. Relationship between resultant normal reaction force from subsoil and relative location of its application for gravity type RW

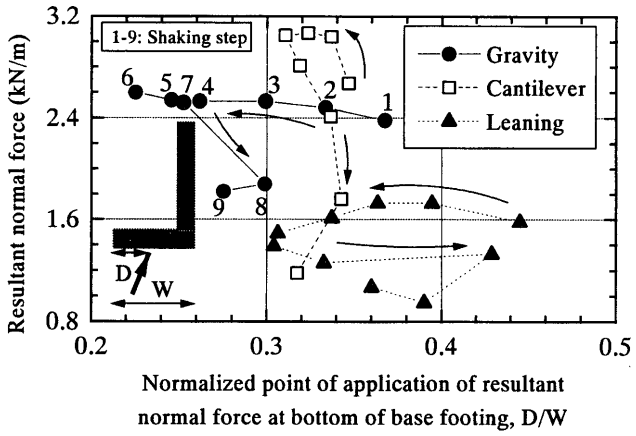

Fig. 20. Comparison of resultant normal reaction force from subsoil and relative location of its application

and the edge of the toe of the base footing, and W is the width of the base footing. On the early shaking steps (at the 1st through 6th shaking steps in Fig. 18), the normal stress increased rapidly at the toe of the base footing (LT7), while it decreased at the heel of the footing (LT4). At these shaking steps, the application point of the resultant force gradually moved toward the toe of the base footing, accompanied by only a slight increase in the amount of the resultant normal force (Fig. 19). After attaining the peak state of the normal stress at the toe of the base footing (LT7), the d_{top} value suddenly increased due to the loss of bearing capacity near the toe of the base footing (at the 7th through 9th shaking steps in Fig. 18). At these shaking steps, the resultant normal force decreased suddenly, and its application point moved back toward the heel of the base footing (Fig. 19). This behavior caused a large decrease in the resistance moment against overturning, which led to low ductility of the gravity type RWs.

Figure 20 compares the relations between the resultant normal force from subsoil and relative location of its application among the three conventional type RWs. A similar trend was observed among them. That is, before the loss of bearing capacity, the resultant normal force did not change largely and its application point gradually moved toward the toe of the base footing. After the local bearing capacity failure at the toe of the base footing, on the other hand, the resultant normal force suddenly decreased, and its application point moved back toward the heel of the base footing.

It can also be seen from Fig. 20 that the reduction in the D/W value of the cantilever type RW before local bearing capacity failure was to a much lesser extent than that of other RWs. This may be due to the mobilization of a large shear stress along the vertical failure plane developed from the heel of the cantilever type RW that could reduce the overturning moment acting on the base footing (Fig. 21).

In a number of the current design procedures, the seismic stability against overturning of RWs and bearing capacity failure of subsoils below RWs are analyzed independently with the interaction not taken into account. On the other hand, the current design standard for railway foundations and soil retaining structures in Japan (R.T.R.I., 2000b) is based on the limit state design, which takes into consideration the gradual movement of the application point of the resultant force toward the toe of the base footing before the occurrence of bearing capacity failure. However, the standard does not consider the movement of the application point of the resultant force back toward the heel of the base footing after bearing capacity failure as observed in Fig. 20. In order to predict the residual deformation of RWs rationally, such behavior should be considered properly.

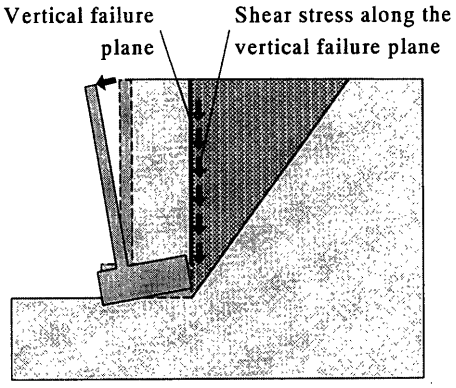

Fig. 21. Shear stress mobilized along the vertical failure plane for the cantilever type RW

Seismic Stability of Reinforced-Soil RWs

As mentioned above in regard to Fig. 10, the rate of accumulation of the d_{top} value did not increase rapidly for any of the three types of reinforced-soil RWs. The reinforced-soil RWs resist the overturning moment mainly by the tensile force in the reinforcements as shown in Fig. 1. Figure 22 shows the time history of tensile force in several reinforcement layers which were measured at a horizontal distance of 2.5 cm from the facing in the uppermost, middle-height and lowest layers for the reinforced-soil type 2 RW during a shaking step when a_{max} was equal to 519 gal. All tensile forces increased almost simultaneously to resist the overturning moment when the inertia force was oriented outward, the point A in Fig. 22.

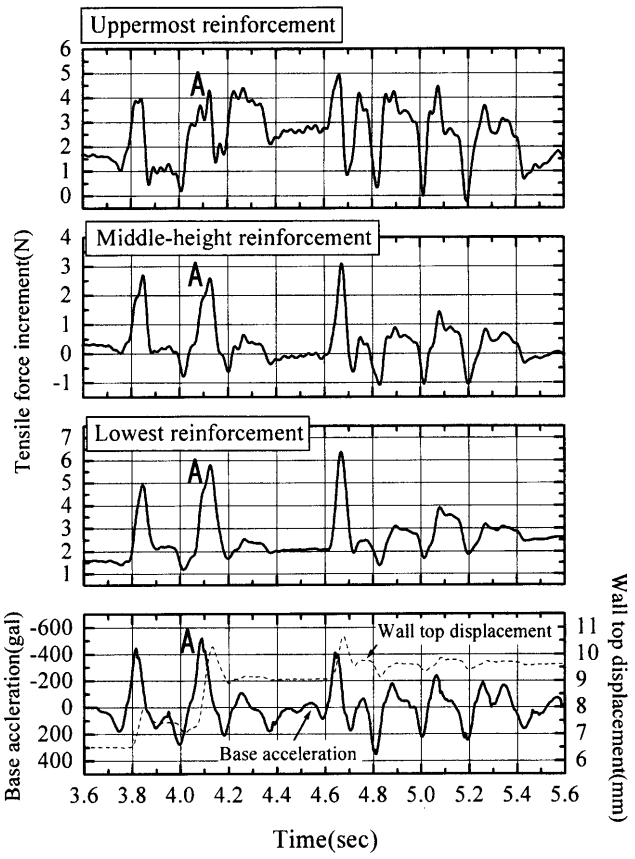

Fig. 22. Time history of tensile force in reinforcement for reinforced-soil type 2 RW

Figure 23 shows the relation between the tensile force and the wall top horizontal displacement d_{top}. The tensile force was evaluated when the base acceleration inducing outward inertia force became its maximum in each shaking step. For all types of reinforced-soil RWs, the tensile force increased as the d_{top} value increased, not showing such a sudden drop as observed in the reaction force from subsoil for the gravity type RW (Fig. 18). This may explain the ductile behavior of reinforced-soil RWs.

It can also be seen from Fig. 23 that the tensile force in the uppermost layer was the largest for the reinforced-soil type 2 RW with the longest reinforcement, while it was the smallest for the reinforced-soil type 1 RW with the shortest reinforcement. In particular, the former value increased even when the d_{top} value was relatively small, while the latter value increased only after the d_{top} value exceeded about 20 mm. This difference may have been caused by the location of the failure plane relative to the reinforcement. Figure 24 shows the location of the failure planes and the reinforcements for reinforced-soil type 2 RW. The two failure planes formed almost simultaneously, and the arrows in Fig. 24 indicate the end location of longer reinforcements at the moment when the failure planes formed. The upper failure plane developed from the back of the reinforced zone toward just beside the end of the extended reinforcement ($L=45$ cm), and stopped somewhere below the longest reinforcement. On the other hand, the lower failure plane formed just beside the end of the longest reinforcement ($L=80$ cm). This demonstrates that the reinforcement resisted the formation of the failure plane, and the location of the failure plane was strongly governed by the existence of the extended reinforcement. Accordingly, large tensile force was mobilized in the uppermost extended reinforcement of the reinforced-soil type 2 RW as shown in Fig. 23, although the confining pressure was relatively low. This result may suggest that the extension of upper reinforcement layer, such as the case of reinforced-soil type 2 RW, effectively mobilizes the tensile force in the extended reinforcement. This method is recommended to effectively increase the seismic stability of reinforced-soil RW.

On the other hand, at the mid-height reinforcement layer of the type 2 RW, the tensile force was not largely mobilized compared with the type 3 RW even though it was extended to 45 cm. This may be caused by the concentration of the mobilized tensile force in the extended uppermost reinforcement. This indicates that the height of reinforcement where the largest tensile force would be mobilized may depend on the arrangement of reinforcement.

Figures 25(a), (b) and (c) show the horizontal distribution of tensile force in each reinforcement. As the facing was rigid, almost all tensile forces were maximized at a point nearest the facing. For the reinforced-soil type 2 RW, however, the tensile force in the uppermost reinforcement ($L=80$ cm) was constantly large showing a reduction with approaching its tip. Such different degrees of

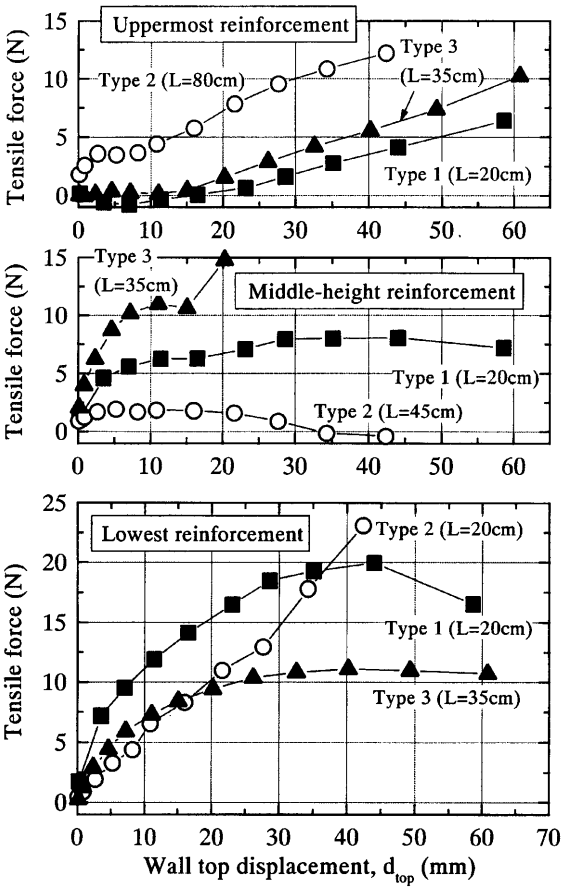

Fig. 23. Tensile forces in reinforcement layers measured at a distance of 2.5 cm from facing of reinforced-soil RWs

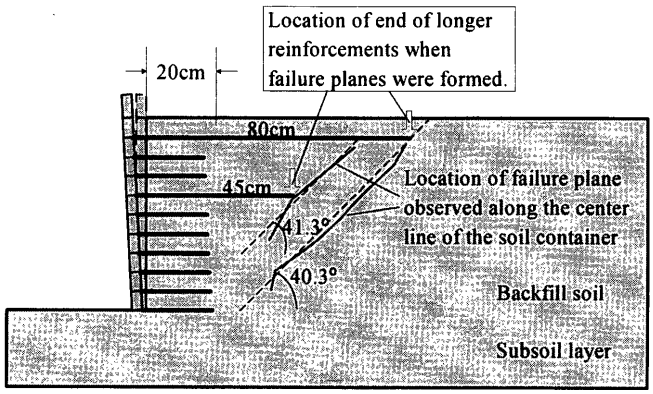

Fig. 24. Comparison of locations of failure planes and longer reinforcement layers for reinforced-soil type 2 RW

mobilization of tensile force may be linked to the different locations of these reinforcements relative to the failure planes as typically shown in Fig. 24. That is, the tensile force in the uppermost reinforcement for the reinforced-soil type 2 RW was largely mobilized to resist the formation of the upper failure plane which would have otherwise reached the surface of the backfill.

As shown in Fig. 4, phosphor-bronze strips were used as the model reinforcement so that the tensile force mobilized in the reinforcement could easily be measured. When compared with the actual geosynthetics used for reinforcement layers, however, the stiffness of phosphor-bronze is too high. As the horizontal and vertical distribution of tensile force may be affected by the stiffness and the strength of the reinforcement, further investigations are required on the effect of these properties.

Stability Analysis of RW Models

The safety factors against overturning, sliding and bearing capacity failure of the RW models were evaluated based on the limit equilibrium method with the pseudo-static approach. For each test, the critical seismic coefficient $(k_h)_{cr}$ was defined at the state where the calculated safety factor became equal to unity. Theoretical lateral earth pressures acting on the backface of the wall were calculated by the Mononobe-Okabe method (Okabe, 1924; Mononobe and Matsuo, 1929) assuming a single soil wedge for the conventional walls and by the two-wedge method for the reinforced-soil type walls, as described by Horii et al. (1994). In both methods, earth pressures due to the self-weight of the backfill were assumed to be hydrostatically distributed along the wall height, and those due to the surcharge applied at the top of the backfill were assumed to be uniformly distributed. This assumption of hydrostatic distribution was adopted because it is widely used in the current practice to design retaining walls in Japan.

The theoretical safety factors against overturning were obtained by assuming that overturning occurred around the toe of the base part of the wall. The bearing capacity of the conventional walls was evaluated by assuming that the subsoil thickness was sufficient to cause boundary-free subsoil failure, despite the fact that the actual thickness of subsoil layer was limited to 200 mm.

For the cantilever wall having a wall base overlain by the backfill, a virtual vertical backface was assumed within the backfill, and the portion of the backfill located above the wall base and between the backface of facing and the virtual backface was regarded as a part of the wall.

The shear resistance angle ϕ of the backfill and subsoil layers was set equal to ϕ_{peak} (=51 degrees) obtained from the relevant plane strain compression (PSC) tests (Koseki et al., 1998a).

It is very likely that the friction angle along the bottom face of the rigid base is equivalent to the simple shear angle of friction $\phi_{ss} = \arctan(\tau/\phi)_{max}$ along the horizontal failure plane. A value of around 3/4 was obtained as the ratio of the simple shear peak friction angle ϕ_{ss} to the peak angle of $\phi_{peak} = \arcsin\{(\sigma_1-\sigma_3)/(\sigma_1+\sigma_3)_{max}\}$ from the PSC tests having the vertical σ_1 direction, both obtained for air-pluviated Toyoura sand (Tatsuoka et al., 1991). When the effect of the sand paper glued on the surface of the wall base was considered, the frictional angle δ_b at the interface between the subsoil and the wall base was assumed to be equal to 3/4 ϕ_{peak} (=38 degrees) in the calculation of the safety factor against sliding.

Similarly, ignoring the effects of strength anisotropy, the frictional angle δ_w at the interface between the backfill

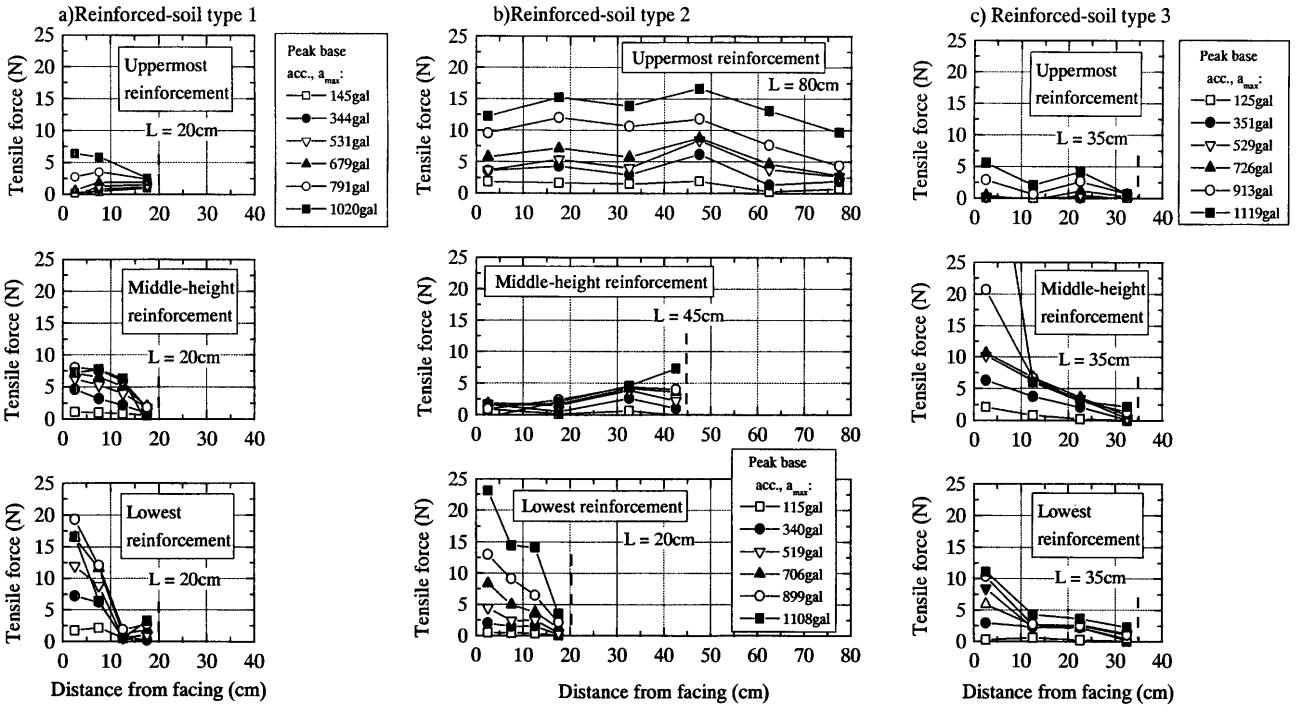

Fig. 25. Horizontal distribution of tensile forces in reinforcement layers for reinforced-soil retaining walls: a) type 1, b) type 2 and c) type 3

and the wall facing with sand paper was set equal to 3/4 ϕ_{peak}. For the cantilever type wall, the δ_w value along the assumed virtual vertical backface was also set equal to 3/4 ϕ_{peak}, because the safety factor equal to unity could not be obtained until the seismic coefficient became unrealistically large when δ_w was set equal to ϕ_{peak}.

These evaluation procedures of RW stability did not consider the dynamic effects in the shaking table tests, such as amplification and phase lag between the response and the base accelerations, or the effects of progressive failure.

Figure 26 shows the relations between the observed critical seismic coefficient $(k_h)_{ult}$ for the ultimate overall wall failure and the calculated values of $(k_h)_{cr}$ against external instability obtained for the observed major failure pattern (i.e., overturning or bearing capacity failure).

The observed values of $(k_h)_{ult}$ were obtained based on the relations between the seismic coefficient k_h and the wall top horizontal displacement d_{top}. As shown in Fig. 10, the d_{top} value increased very rapidly in the sinusoidal shaking tests and the tilting tests, after exceeding about 25 mm that corresponds to about 5% of the total wall height, soon resulting in the ultimate overall wall failure. The values of $(k_h)_{ult}$ are defined, therefore, as the value when the d_{top} value exceeded 5% of the wall height.

The calculated value of $(k_h)_{cr}$ for conventional type RWs was obtained from the smaller value of the calculated critical seismic coefficient against bearing capacity failure or against overturning. It should be noted that, for reinforced-soil RWs, the bearing capacity failure was not considered in the calculation of $(k_h)_{cr}$, since the wall can maintain its stability even when the load acting at the bottom of the facing reaches the bearing capacity of the subsoil, as has been demonstrated by a large-scale shaking test on a similar model of reinforced-soil RW (Murata et al., 1994). It should be reminded that the bearing capacity of the conventional RWs was evaluated by assuming that the subsoil thickness was sufficient to cause boundary-free subsoil failure despite the fact that the actual thickness of the Toyoura sand layer was only 200 mm (Fig. 3). Therefore, the safety factors against bearing capacity failure may have been somehow underestimated. In Fig. 26, this inference is indicated by arrows directing right shown next to the data points for the cantilever and gravity type RWs.

The following trends may be seen from Fig. 26:

1) The base width was the same, equal to 230 mm, among the gravity and cantilever type RWs and the reinforced-soil type 1 RW (if the reinforced backfill is regarded as a part of the base). On the other hand, for the leaning type RW, the base width was 180 mm, whereas the width between the top of the backface and the toe of the base was wider, equal to 330 mm. Despite the above conditions, in the tilting tests, the reinforced-soil type 1 RW and the cantilever RW had larger values of $(k_h)_{ult}$ than those of the leaning type and gravity type RWs. In the sinusoidal and irregular shaking tests, the reinforced-soil type 1 RW was more stable than the others. These results are, in a broad sense, consistent with the full-scale field behavior observed during the Hyogoken-Nambu earthquake (Tatsuoka et al., 1996), suggesting a relatively high seismic stability of reinforced-soil RWs having a full-height rigid (FHR) facing.
2) In the tilting tests, the ratios $(k_h)_{ult}/(k_h)_{cr}$ were gener-

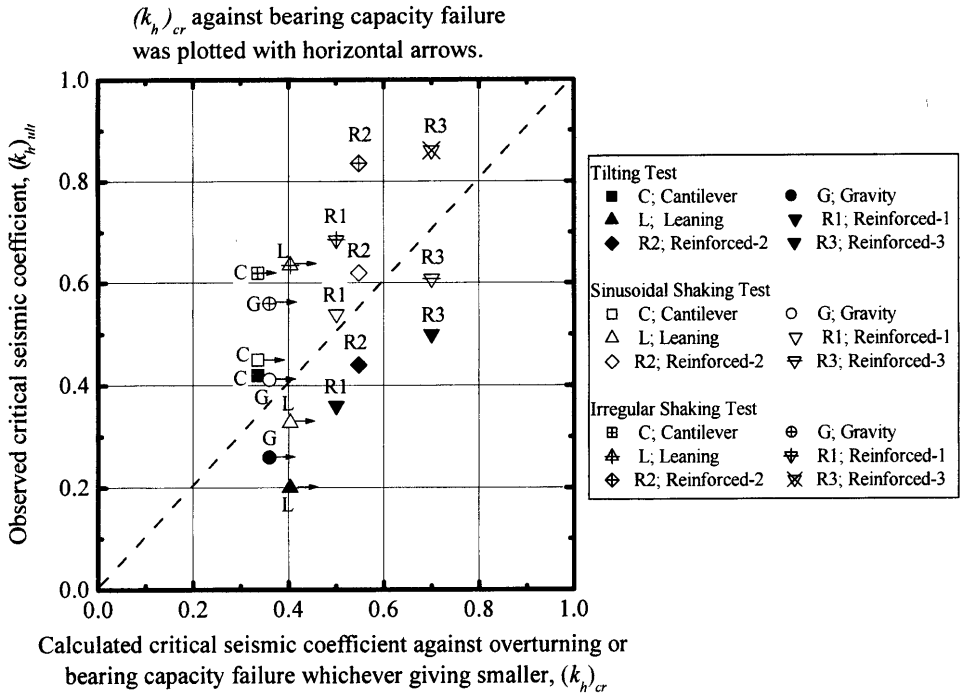

Fig. 26. Comparison of observed critical seismic coefficients to calculated ones against overturning or bearing capacity failure

ally lower than unity, perhaps except for the cantilever type RW. This result suggests that the stability of RW is over-estimated by the conventional pseudo-static approaches using the peak soil strength ϕ_{peak} obtained under plane strain conditions with the σ_1 direction normal to the bedding plane direction. This overestimation is possibly due to the fact that the effects of progressive failure associated with strain softening properties are not considered in the pseudo-static approaches.

3) In the sinusoidal shaking tests, the ratios $(k_h)_{ult}/(k_h)_{cr}$ were generally larger than unity, except for the leaning and reinforced-soil type 3 RWs. These ratios were larger than those observed in the tilting tests. In the irregular shaking tests, the ratios $(k_h)_{ult}/(k_h)_{cr}$ were larger than those observed in the sinusoidal shaking tests. In addition, these ratios were different among the different types of RWs. These facts suggest that the dynamic stability of RWs is not totally controlled by "peak base acceleration" devided by g, but also by other dynamic factors such as the duration of peak lateral force acting on the backface of wall, phase lag and amplification of response acceleration, dynamic ductility and flexibility of RWs, and dynamic shear deformation of backfill, especially for the reinforced-soil type RWs with longer reinforcements. Effects of those dynamic factors should not be ignored for proper seismic stability analysis of RWs.

4) In the sinusoidal and irregular shaking tests, the values of $(k_h)_{ult}$ were similar for the reinforced-soil type 2 RW having a couple of long reinforcement layers at high levels in the backfill and the reinforced-soil type 3 RW having moderately long same-length reinforcement layers. On the other hand, the total amount of reinforcements was smaller for the reinforced-soil type 2 RW, and the values of $(k_h)_{cr}$ were also smaller for this type 2 RW. When reinforced-soil RWs having a FHR facing are constructed on existing slopes, the use of relatively short reinforcements at low levels is preferred to minimize the amount of slope excavation. Based on the test results described above, using several long reinforcement layers at high levels, as the reinforced-soil type 2 RW, can be recommended to effectively increase RW seismic stability.

CONCLUSION

A series of model shaking and tilting tests were carried out on different types of retaining walls, and the following conclusions were drawn.

1. In the irregular shaking tests on leaning type and gravity type RWs, after a failure plane formed in the backfill, a second failure plane formed at higher seismic loads. This can be explained by the effects of strain localization in the backfill soil and associated post-peak reduction in the shear resistance from peak to residual values along the previously formed failure plane.
2. The residual displacement of each model wall was larger in the order of tilting test, sinusoidal shaking test and irregular shaking test. This is mainly due to the different durations of the peak seismic load among these tests.
3. At high seismic loads, reinforced-soil type RWs showed a more ductile behavior than the convention-

al (cantilever, gravity and leaning) type RWs. When the model walls started to tilt, concentration of subsoil reactions at the toe of conventional type RWs resulted in local failure due to the loss of bearing capacity. On the other hand, under similar conditions, tensile force in the reinforcement of the reinforced-soil RWs could be mobilized effectively to resist the wall movement.

4. In the static tilting tests, the observed critical seismic coefficient at the ultimate overall wall failure was smaller than that calculated by the Mononobe-Okabe method using ϕ_{peak}. This is possibly due to the effects of progressive failure with strain softening in the backfill, which are not considered in the calculation. On the other hand, in irregular shaking tests, the observed seismic coefficient at the ultimate overall wall failure was the largest for the same type of RW. This is possibly affected by several dynamic factors such as different durations of the peak seismic load, phase lag and amplification of response acceleration, dynamic ductility and flexibility of RWs, and dynamic shear deformation of backfill.
5. It was demonstrated that extension of several upper reinforcements improved effectively the seismic stability of reinforced-soil walls. This is because the tensile force in the extended reinforcement was largely mobilized to resist the formation of the failure plane. On the other hand, effects of shear deformation of the reinforced backfill, which are not considered in the current design procedures, cannot be ignored, in particular for reinforced-soil RWs with longer reinforcements.
6. The effect of the side wall friction of the soil container on the response acceleration of the backfill and the angle of failure plane measured along the center line of soil container was confirmed to be negligible. It was also confirmed that the failure plane observed through the transparent side wall and along the center line of the soil container formed almost simultaneously.

ACKNOWLEDGEMENT

The authors appreciate the assistance of Professor Tatsuoka, F., Professor of Department of Civil Engineering, University of Tokyo, for his valuable suggestions on our research; Mr. Sato, T., Research Associate at the Institute of Industrial Science, University of Tokyo, for his thoughtful suggestions and discussions on the method of performing the model tests; Mr. Ebisawa, S. and Mr. Morikoshi, S. at Alfa Engineering Co., Ltd. for their assistance in conducting the model tests and Mr. Horii, K. of Integrated Geotechnology Institute Limited, for his great help in performing the stability analysis of the reinforced-soil type RWs.

REFERENCES

1) Bathurst, R. J. and Alfaro, M. C. (1996): Review of seismic design, analysis and performance of geosynthetic reinforced walls, slopes and embankments, *Proc. of Int. Symp. on Earth Reinforcement* (eds. by Ochiai, H. et al.), Balkema, **2**, Keynote lecture, 887–918.
2) Horii, K., Kishida, H., Tateyama, M. and Tatsuoka, F. (1994): Computerized design method for geosynthetic-reinforced soil retaining walls for railway embankments, *Recent Case Histories of Permanent Geosynthetic-Reinforced Soil Retaining Walls* (eds. by Tatsuoka and Leshchinsky), Balkema, 205–218.
3) Koseki, J., Munaf, Y., Tatsuoka, F., Tateyama, M., Kojima, K. and Sato, T. (1998a): Shaking table and tilt table tests of geosynthetic-reinforced soil and conventional retaining wall, *Geosynthetics Int.*, **5** (1–2), 73–96.
4) Koseki, J., Tatsuoka, F., Munaf, Y., Tateyama, M. and Kojima, K. (1998b): A modified procedure to evaluate active earth pressure at high seismic loads, *Soils and Foundations*, Special Issue on Geotechnical Aspect of the January 17 1995 Hyogoken-Nambu Earthquake, (2), 209–216.
5) Koseki, J., Munaf, Y., Tateyama, M., Kojima, K. and Horii, K. (1999): Back analyses of case histories and model tests on seismic stability of retaining walls, *11th Asian Regional Conf. on Soil Mechanics and Geotech. Engrg.*, **1**, 399–402.
6) Mononobe, N. and Matsuo, H. (1929): On determination of earth pressure during earthquake, *Proc. World Engrg. Congress*, Tokyo, **9**, 177–185.
7) Murata, O., Tateyama, M. and Tatsuoka, F. (1994): Shaking table tests on a large geosynthetic-reinforced soil retaining wall model, *Recent Case Histories of Permanent Geosynthetic-reinforced Soil Retaining Walls* (eds. by Tatsuoka and Leshchinsky), Balkema, **1**, 259–264.
8) Okabe, S. (1924): General theory on earth pressure and seismic stability of retaining wall and dam, *J. of Japan Soc. of Civil Engineers*, **10** (6), 1277–1323.
9) Railway Technical Research Institute (2000a): *Railway Structure Design Standard for Earth Structures (SI unit version)*, Maruzen, 158–159 (in Japanese).
10) Railway Technical Research Institute (2000b): *Railway Structure Design Standard for Foundations and Soil Retaining Structures (SI unit version)*, Maruzen, 130–135 (in Japanese).
11) Sakaguchi, M. (1996): A study of the seismic behavior of geosynthetic reinforcement walls in Japan, *Geosynthetics Int.*, **3** (1), 13–30.
12) Tatsuoka, F., Okahara, M., Tanaka, T., Tani, K., Morimoto, T. and Siddiquee, M. S. A. (1991): Progressive failure and particle size effect in bearing capacity of a footing on sand, *Geotech. Engrg. Congress 1991*, ASCE, Geotech. Special Publication, **2** (27), 788–802.
13) Tatsuoka, F., Tateyama, M. and Koseki, J. (1996): Performance of soil retaining walls for railway embankments, *Soils and Foundations*, Special Issue of Soils and Foundations on Geotechnical Aspects of the January 17 1995 Hyogoken-Nambu Earthquake, 311–324.
14) Whitman, R. V. (1990): Seismic design and behavior of gravity retaining walls, *Design and Performance of Earth Retaining Structures*, Geotechnical Special Publication ASCE, (25), 817–840.